The Cryosphere Discuss., 9, 5413–5443, 2015
www.the-cryosphere-discuss.net/9/5413/2015/
doi:10.5194/tcd-9-5413-2015

The Cryosphere Discussions
Open Access

Wind tunnel experiments: cold-air pooling and atmospheric decoupling above a melting snow patch

R. Mott[1], E. Paterna[1], S. Horender[1], P. Crivelli[1], and M. Lehning[1,2]

[1]WSL Institute for Snow and Avalanche Research SLF, Davos, Switzerland
[2]School of Architecture, Civil and Environmental Engineering, Laboratory of Cryospheric Sciences (CRYOS), Ècole Polytechnique Fèdèrale de Lausanne, Lausanne, Switzerland

Received: 23 July 2015 – Accepted: 15 September 2015 – Published: 8 October 2015

Correspondence to: R. Mott (mott@slf.ch)

Published by Copernicus Publications on behalf of the European Geosciences Union.

Abstract

The longevity of perennial snow fields is not fully understood but it is known that strong atmospheric stability and thus boundary layer decoupling limits the amount of (sensible and latent) heat that can be transmitted to the snow surface. The strong stability is typically caused by two factors, (i) the temperature difference between the (melting) snow surface and the near-surface atmosphere and (ii) cold-air pooling in topographic depressions. These factors are almost always a prerequisite for perennial snow fields to exist. For the first time, this contribution investigates the relative importance of the two factors in a controlled wind tunnel environment. Vertical profiles of sensible heat fluxes are measured using two-component hot wire and one-component cold-wire anemometry directly over the melting snow patch. The comparison between a flat snow surface and one that has a depression shows that atmospheric decoupling is strongly increased in the case of topographic sheltering but only for low to moderate wind speeds. For those conditions, the near-surface suppression of turbulent mixing was observed to be strongest and drainage flows were decoupled from the surface enhancing atmospheric stability and promoting the cold-air pooling over the single snow patch. Further work is required to systematically and quantitatively describe the flux distribution for varying terrain geometry, wind speeds and air temperatures.

1 Introduction

Snow cover can be highly heterogeneous on various scales, introducing inhomogeneities in surface characteristics such as surface albedo, roughness or temperature (Essery, 1997). Once an alpine snow cover gets patchy in spring, steps in surface roughness and surface temperature induce the development of thermal internal boundary layers. Increasing air temperatures in spring cause stable internal atmospheric layers above the melting snow-covered surface. The stability is further enhanced by the forced flow of warm air advected by the mean wind from the snow-free land over the colder snow-covered areas changing the atmospheric boundary layer characteristics over snow by increasing the local air temperature there. The complex interactions between snow, bare ground and atmosphere strongly affect the energy balance at the snow surface, thus snow melt and runoff in spring. Typically, hydrological and energy balance studies do not account for those processes involved because they rely on the existence of constant flux layers and simply apply bulk transfer models. Only a small number of investigations on processes driving snow melt that are affected by the development of thermal internal boundary layers exist so far (Essery, 1997; Neumann and Marsh, 1998; Essery et al., 2006; Granger et al., 2006; Mott et al., 2013, 2015).

Another phenomenon that is directly linked to the existence of stable internal boundary layer development is the formation of cold-air pools driving the survival of perennial snow fields (Fujita et al., 2010). Cold air pools typically develop in closed sink holes, topographical depressions or narrow valleys (Whiteman et al., 2001; Vosper et al., 2014). They either develop due to drainage flows (Whiteman et al., 2008; Bodine et al., 2006) or due to sheltering effects (Gustavsson et al., 1998; Bruns and Chemel, 2014). Sheltering effects and in situ cooling are typically described for small-scale valleys (i.e. 100 m deep and up to 3 km wide), where the valley air is decoupled from the atmospheric boundary layer above due to the sheltering effect of valley geometry (Price et al., 2011). Sheltering causes reduced turbulence and prevents heat transfer from above, allowing the valley atmosphere to cool by radiative heat loss (Bruns and Chemel, 2014). The sheltering effect is enhanced by strong atmospheric stabilities that are typically connected with calm wind conditions and boundary layer decoupling is promoted (Vosper et al., 2014). A special case is cold-air pooling over snow fields that are located within topographical depressions and where associated atmospheric decoupling is mainly driven by the cooling effect of the underlying snow on the air. This phenomenon, however, has gained little attention so far (Fujita et al., 2010). Long-lasting snow patches are typically located within topographical depressions because snow is preferentially accumulated in sheltered areas (Tabler, 1975; Winstral et al., 2002; Lehning et al., 2008; Mott et al., 2010, 2014; Dadic et al., 2010) and the snow is well protected within topographical depressions due to lower wind speeds decreasing turbulent fluxes (Mott et al., 2011a). For low wind speeds, the cooling effect of the snow and advective transport of warm air increase the local atmospheric stability and promote cold-air pooling and atmospheric decoupling above snow patches (Fujita et al., 2010; Mott et al., 2013).

The mean perimeters of snow patches in alpine terrain are typically in the range of tens to hundreds of meters. The formation of shallow cold-air pools and connected atmospheric decoupling above small-scale snow patches is difficult to measure or to simulate with a numerical model (Mott et al., 2015). In the field, atmospheric profiles obtained from eddy-correlation measurements are typically based on a few measurement points, which makes it difficult to capture boundary layer dynamics of shallow internal thermal boundary layers. Especially turbulent heat fluxes close to the snow surface are difficult to measure in the field because of the relatively large path lengths of sonic anemometers. Measurement results, thus, only give a rough estimate on boundary layer dynamics close to the surface. Numerically, high horizontal resolution of at least 5 m are necessary to adequately represent the formation of thermal internal boundary layers. What cannot be captured with that resolutions is the strong suppression of turbulence due to strong atmospheric stability at the lowest centimeters above the snow surface (Mott et al., 2015). Wind tunnels provide optimal conditions to measure the boundary layer dynamics above cooled surface (Ohya, 2001; Ohya et al., 2008). The wind tunnel not only allows us to measure boundary layer dynamics under controlled conditions, but the available measurement techniques also allow us at the expense of reduced eddy sizes and reduced directional variability to measure vertical profiles of turbulent quantities with a high vertical resolution of approximately 0.005 m (normalized by boundary layer height in the wind tunnel z/δ this means 0.016). Measurements conducted in the wind tunnel are thus expected to advance our understanding of the flow field development and the associated heat exchange when the flow crosses a single snow field. Earlier wind-tunnel studies of the atmospheric stable boundary layer were conducted using a thermally stratified wind tunnel (Ohya, 2001; Ohya et al., 2008). For those experiments, stably stratified flows were generated by heating the wind tunnel airflow and cooling the test-section floor, creating high temperature differences between air and floor up to 40 °C and bulk Richardson numbers larger than 1. In our experiments, the warmer air within the wind tunnel flows across a snow patch creating a shallow stable layer with smaller temperature differences up to 14 °C, which are typical for spring conditions when snow melts in higher altitudes (Mott et al., 2011a).

In this experimental study we investigate the development of the atmospheric boundary layer when the boundary layer flow crosses a single snow patch. The purpose of this study is to examine boundary conditions for cold-air pooling and atmospheric boundary layer decoupling over seasonal snow patches or perennial snow fields. The experimental setup accounts for the effect of synoptic wind forcing and the effect of the topography. With this setup we want to look into the relative role of topographic sheltering vs. temperature differences in the generation of decoupling and stratification over snow patches.

2 Methods and data

2.1 Experimental methods

All experiments conducted for that study are listed in Table 1. Measurements were performed in the SLF boundary layer wind tunnel (Fig. 1) in Davos in a non-heated building at 1650 m a.s.l. The wind tunnel is an open-circuit suck-down type and 17 m long and has a cross section of 1 m × 1 m. In the upwind part of the wind tunnel the boundary layer flow was preconditioned by spires and additional roughness elements, that were arranged along a 6 m long fetch. In the middle Sect. 6.4 m of wooden plates featured a smooth surface. The measurement section was located at the downwind end of the wind tunnel, consisting of a 1.6 m long snow patch. The surface shape of the snow patch was either flat (Experiment E1) or concave (Experiment E2). The concave has a length (l) of 1.6 m and a maximum depth (z_{max}) of 0.1 m. These dimensions

($z_{max} : l = 0.06$) were defined to scale with a cavity in the Wannengrat catchment ($z_{max} : l = 2.5 : 60 = 0.04$), that was studied by Mott et al. (2013) revealing boundary layer decoupling above a melting snow field. For experiments E1 and E2 profiles of mean and turbulent quantities were measured at 0.4 m (X1) and 0.8 m (X2) downwind of the leading edge of the snow patch. For E2, the depth of the snow-covered depression is 0.06 m at X1 and 0.1 m at X2. All experiments were performed at free-stream wind velocities of approximately 1, 2 and 3 m s^{-1} (V1, V2, V3). All heights are given relative to Z0, which is the height of wooden floor and the initial snow cover at fetch distance 0. For the concave setup, Z0 corresponds to the topographical step height. Consequently, for the concave setup E2 the snow surface belongs to $z = -0.06$ m at X1 and to $z = -0.1$ m at X2. Please note that due to the configuration of the probes, we were able to measure closer to the ground for the flat setup (E1) than for the concave setup (E2). While the lowest measurement point above snow is approximately 0.002 m for E1 it is 0.01 m for E2. Furthermore, the snow surface temperature was at its melting point during the whole experiment, resulting in a change of the snow surface during the experimental period. As a consequence of the melting snow surface, the heights above the snow surface are not consistent throughout the experimental period. Thus, not only profiles of E2, but also of E1V2 and E1V3 feature negative heights.

The temperature and velocity fluctuations were measured simultaneously using a system of a two-component platinum coated hot-wire anemometer (TSI 1240-60) and a one-component cold-wire anemometer (Dantec 55P11). The calibration was performed in situ before each test against a calibrated miniature fan anemometer (Schiltknecht MiniAir20) for the velocity measurements and against a digital thermometer (Labfacility Tempmaster-100). Data were acquired at a frequency of 1 kHz and for 100 s during the tests on setup 1 and 20 s during the tests on Experiment 2 (E2). The data were low-pass filtered by means of a butterworth filter with a cut-off frequency of 100 Hz. Furthermore, to eliminate low-frequency trends in the signal data were also high-pass filtered with a cut-off frequency of 0.2 Hz. Being the tests conducted at low velocities a threshold was applied based on the Reynolds (the ratio of momentum

TCD
9, 5413–5443, 2015

Atmospheric boundary layer flow above a single snow patch

R. Mott et al.

forces to viscous forces) and Grashof number (the ratio of the buoyancy to viscous forces) to eliminate velocity data significantly influenced by the natural convection of the wire (Collis and Williams, 1958). The time-series exceeding the latter threshold for more than 10 % of the time were not considered for the following analysis. Following this procedure four points in total have been removed from the data set.

2.2 Quadrant analysis

Quadrant analysis consists of conditionally averaging the shear stresses into four quadrants depending on the sign of the streamwise and vertical velocity fluctuations (Wallace et al., 1972). The resulting types of motions are following the description in Table 2: outward motion of high-momentum fluid (Q1) where $u' > 0$ and $w' > 0$, ejections of low-momentum fluid (Q2) where $u' < 0$ and $w' > 0$, wallward interactions of fluids from the wall (Q3) where $u' < 0$ and $w' < 0$ and sweeps of high-moment fluid towards the wall (Q4) where $u' > 0$ and $w' < 0$. Here u and w correspond to streamwise and vertical velocity and primes indicate the deviation from the average value. Each quadrant event $\langle u'w' \rangle_i$ can be defined as:

$$\langle u'w' \rangle_i = \lim_{T \to \infty} \frac{1}{T} \int_0^T u'(t) w'(t) \mathrm{d}t \qquad (1)$$

where T is the length of the time-series and i marks the quadrant event ($i = 1, \ldots, 4$). While Q1 and Q3 motions are positive stress producing motions, ejections and sweeps contribute positively to the Reynolds stress. The negative contributions by Q1 and Q3 motions corresponds to the interaction between ejection and sweep motions. In neutrally stratified boundary layer flows, the main contributions to the Reynolds stress comes from sweep and ejection motions and both motions are nearly equal (Wallace et al., 1972).

In our case all the events from each quadrant are considered and no event is discarded based on its magnitude. Therefore the analysis concentrates on the overall flow dynamics rather than focusing on the strength of the motions. The second (ejections) and fourth (sweeps) quadrants constitute a positive contribution to the production of turbulent kinetic energy and to the momentum flux towards the surface, while the other two constitute a negative contribution.

3 Results

3.1 Experimental conditions

The flow conditions for each experimental case are listed in Table 1. The free-stream wind velocity U_∞ ranged between 0.9 and 3.3 $\mathrm{m\,s^{-1}}$ with ambient air temperaturesranging between 11.8 and 14.1 °C. The snow surface temperature was 0 °C for all experiments. Since, the flow first crossed a smooth wooden floor before crossing a flat (E1) or concavely shaped (E2) snow patch, the flow was streamwise inhomogeneous. The bulk Richardson numbers, defined as a dimensionless number relating vertical stability and vertical shear, are below the critical value of 0.25 for all profiles. That means that the flow is expected to be dynamically unstable and turbulent. For both setups, the bulk Richardson number (Ri_{bulk}) was slightly higher at X2 than at X1 due to a slightly stronger cooling of the atmosphere further downwind. While the flow for the experimental cases with low free-stream wind (V1) was statically stable with Ri_{bulk} numbers ranging between 0.19 and 0.22, experimental cases driven by higher free-stream wind velocities (V2, V3) show low Ri_{bulk} numbers ranging between 0.02 and 0.05.

3.2 Vertical profiles of mean quantities

The vertical profiles of the streamwise wind velocity U and mean air temperature T are illustrated in Fig. 2 for the different experimental cases and fetch distances. The mean air temperature is normalized by the difference between the ambient air temperature T_∞ and the surface temperature T_s (which was 0 °C throughout the measurements). The mean wind velocity U is normalized by the free-stream wind velocity U_∞.

TCD
9, 5413–5443, 2015

The temperature profiles show stably stratified flows, that are generated above the snow patch at fetch distances of X1 and X2. The stable layers are deeper for the concave setup (E2) than for the flat setup (E1). The decrease in air temperature close to the surface is considerably stronger for E1 than for E2, resulting in a stronger local atmospheric stability close to the wall. We have to note, however, that no measurement points are available at the lowest 0.01 m above the surface ($< z = -0.09$ m) for E2. We expect that a higher near-surface measurement resolution for E2 would probably reveal an enhanced temperature gradient below $z = -0.09$ m, at least similar to what we observed for E1 where the highest temperature gradient was found below $z = 0.01$. Over the flat snow patch, the near-surface air temperature gradient is higher at X1 than at X2. Over the concave snow patch, the near-surface air temperature gradient increases in downwind direction revealing colder air at the lowest point of the concave. The thermal boundary layer grows in downwind direction and is deeper for lower wind velocities and for the concave setup.

The velocity profiles of E1 show a weakly pronounced low level jet formed at X2 for low free-stream wind velocity (E1V1). For higher free-stream wind velocities (E1V2, E1V3), the profiles exhibit a gradually increasing wind velocity with height without low level jet evident. The near-surface wind velocities are slightly higher at X2 than at X1. Wind profiles of E2 show a distinct local wind maximum for the low wind velocity case E2V1 and less pronounced for E2V2. For experiments with high free-stream wind velocities (E2V3), the formation of the local wind maximum is not evident anymore. For E2V1, the wind profile at X1 shows a distinct local wind maximum at $z = -0.025$ m relative to the height of the topographical step (Z0) (0.035 m above the local surface). At X2, the wind maximum was measured at $z = -0.05$ m (which corresponds to 0.05 m above the local snow surface). The low-level maxima in velocity (low-level jet) might be caused by the drainage of the cold air along the slope of the cavity. A deep layer of strong wind velocity gradient is visible below the nose of the LLJ (peak of wind velocity). Close to the wall, wind velocities become very small (smaller than 0.2 m s^{-1}) and are much smaller for both distances than measured over the flat snow patch (E1)

TCD
9, 5413–5443, 2015

for a similar ambient wind velocity. The extremely low values of wind velocities within the cavity for the low wind velocity case indicates boundary layer decoupling there. The temperature profiles for the low wind velocity cases are two-layered and show a change of temperature gradient at the height of the respective peaks in wind speed. Similar to the low wind velocity case, temperature profiles of the high wind velocity cases show a strong layering that coincides with the wind velocity profile.

3.3 Vertical profiles of turbulent quantities

Figures 3 illustrates vertical profiles of turbulent momentum flux and vertical turbulent heat flux along the snow patch for the flat and the concave setup. Fluxes are normalized by the free-stream wind velocity and temperature difference between snow surface and ambient air. Figure 4 zooms in on the near-surface profiles (ranging from $z = -0.1$ to $+0.06$ m) of turbulent momentum and vertical turbulent heat flux for the low wind velocity case V1 and the high wind velocity case V3. Primes ($'$) indicate the deviation from the mean value and overbars ($\bar{}$) the average. Momentum fluxes are thus computed as a covariance between instantaneous deviation in horizontal wind speed (u') from the mean value ($\overline{u}$) and instantaneous deviation in vertical wind speed (w') from the mean value ($\overline{w}$). Vertical heat fluxes are computed as a covariance between instantaneous deviation in air temperature (T') from the mean value ($\overline{T}$) and instantaneous deviation in vertical wind speed (w') from the mean value ($\overline{w}$). In theory a thermal internal boundary layer develops with increasing depth in downwind distance as a neutrally stratified flow crosses a single snow patch. Within the stable internal boundary layer turbulent momentum and vertical turbulent heat fluxes are expected to increase with decreasing distance to the snow surface (Essery et al., 2006).

For experiments conducted over the flat snow patch, profiles reveal an increase of negative momentum fluxes with decreasing distance to the snow surface. Contrary, the vertical profiles of turbulent quantities for the concave snow patch (Fig. 4a and c) show a distinct maximum in the negative vertical momentum flux at the height of the shear layer indicating that both, the surface and the high-shear region around $z = 0$ contribute

TCD
9, 5413–5443, 2015

to turbulence generation. For low wind velocities, profiles of momentum fluxes feature a distinct peak approx. 0.04 m above the local surface (Figs. 3 and 4). Below that maximum, momentum fluxes strongly decrease towards the snow surface. This near-surface suppression of momentum flux is strongest further downwind at X2, at the maximum depth of the cavity. The peak of the momentum flux appears to be strongest at the first measurement location downstream of the fetch transition (X1). At the downwind location X2, however, the magnitude of the momentum flux is much lower for the whole profile.

At X1 profiles of the vertical turbulent heat flux reveal a local maximum at $z = +0.02$ m for the flat snow patch with a decrease towards the surface below that maximum (Fig. 4c and d). Further downwind, the maximum heat flux was measured at the lowest point above the surface $z = +0.002$ m) and no suppression of the vertical turbulent heat flux was measured there. On the contrary, for the concave setup, all profiles of heat fluxes feature a similar shape revealing distinct peaks of fluxes at the lowest few centimeters of the atmospheric layer (0.02–0.04 m above the local surface) coinciding with the maximum in vertical velocity fluctuations (not shown). Below that maximum, fluxes strongly decrease towards the snow surface (Fig. 4). The maximum can be found at a higher distance to the ground for the low wind velocity case E2V1, coinciding with maximum wind speed at a height of 0.04–0.05 m above the local snow surface and strong shear in the jet layer (Figs. 2 and 4). Close to the surface, the fluctuation of streamwise and vertical velocity fluctuations are rapidly suppressed at both downwind distances and for all wind velocities. For higher wind velocities, however, the suppression of turbulence is confined to the lowest 0.01–0.02 m of the ABL and is much stronger for the downwind distance X2, where the maximum depth of the cavity is reached.

3.4 Turbulence phenomena at the snow surface

Results from the quadrant analysis are presented for the flat setup E1 (Fig. 5) and the concave setup E2 (Fig. 6). The stress fraction contribution of each quadrant gives insight into the physics of turbulence structures close to the wall (snow cover). In order to discuss the near-surface turbulence in more detail we show the near-surface profiles of mean wind velocity, the vertical momentum and heat fluxes as well as the shear stress distribution for the low and high wind velocity cases at the different measurement locations (Fig. 7). Figure 8 shows the Reynolds number calculated from the local wind velocity at the respective measurement point for experiments E2V1 and E2V3.

For E1 the ejections (Q2) and sweeps (Q4) are observed to dominate the other two events over the whole boundary layer depth (Fig. 5). Both contributions increase with decreasing distance to the wall promoting the downwards directed momentum flux. This result is consistent for all free-stream wind velocities (i.e. experiments E1V1, E1V2, E1V3). This distribution is analogous to the distribution of quadrant motions in neutrally stratified boundary layer flows over flat surfaces, where the ejection-sweep cycle was observed to be induced by coherent flow structures (Adrian et al., 2000).

Over the concave snow patch, ejections and sweeps are observed to dominate over the other two quadrant motions, similarly to the flat case (Fig. 6). In contrast to E1, profiles for E2 reveal a clear dominance of sweeps of high speed fluid downward directed close to the snow surface for all setups, in particular for the lowest wind velocity case where larger stability is also observed (Fig. 5). This marks a clear difference with the distribution of quadrant events for boundary layer flows in neutral stability conditions (see Methods section). The dominance of sweeps close to the wall has therefore to be attributed to the presence of the drainage flows into the concave section (both due to the density and gravity). The presence of drainage flows forming low-level jets is also manifested by the local wind speed maxima defining the nose of the low-level jet (LLJ). The height of the drainage flow varies with wind velocity. At the lowest velocity it is interesting to observe that the peak of both ejections (Q2) and sweeps (Q4) (i.e. the height of the LLJ) occurs at a significantly higher distance from the snow surface than in case of the two other tests at higher velocity.

This is more clearly visible at X2 where the drainage flow is more decoupled from the surface showing the local wind maxima at a higher level at $z = -0.05$ m corresponding

TCD
9, 5413–5443, 2015

to the peak of ejections (Q2) and sweeps (Q4) (Fig. 7e and h). These strong local motions efficiently transport momentum and heat at the height of the drainage flow (Fig. 7f and g). The region below this low level jet corresponds to the cold pool observed in the vertical profiles of heat flux (Fig. 7g and h). The rapid decrease of all strong local motions below the peak at $z = -0.05$ m indicate a strong suppression of turbulent mixing, thus strong atmospheric decoupling over the deepest point of the concave. This is also revealed by the very low Reynolds numbers calculated for measurement points below $z = -0.05$ m that are significantly lower than for the higher wind velocity case indicating laminar flow close to the surface (Fig. 8). These profiles suggest that the higher stability at X2 at the lowest velocity forces the unsteady and coherent flow structures to develop above the cold pool. Moreover, in this latter case such strong reduction of ejections (Q2) and sweeps (Q4) in the cold pool to the level of the other two quadrant events causes the vertical momentum flux to reduce toward zero (Fig. 7f). The strong suppression of high-momentum fluid from the outer region and the strong suppression of turbulent mixing close to the wall (Fig. 8) indicates favorable conditions for cold-air pooling within the cavity, which is strongest at the maximum depth of the cavity (Fig. 7f and g).

For the high wind velocity case, the peak of contributions by Q2 and Q4 motions is shifted towards the wall and the suppression of turbulence is less pronounced and confined to the lowest 0.02 m of the ABL. Over the maximum depth of the cavity, at X2, the peak of Q2 and Q4 motions involve a 0.03 m deep layer of enhanced turbulent mixing (Fig. 7o and p). Thus, with increasing wind velocity gradients towards the wall, sweeps become more dominant towards the snow surface (dominant motion at the lowest points) indicating the rush-in of high speed fluid of the outer layer into the wall region. Furthermore, the strong contribution of Q1 is very conspicuous at X2 and show high values close to the wall. This strong increase of outward interactions (Q1) which are observed to increase with the free-stream velocity (Fig. 7l and p) is a further clear departure from the commonly observed distribution of quadrant motions in neutrally stratified boundary layer flows. The clear dominance of the inner and outward interactions in the concave region indicate that not only turbulence is suppressed but also less organized in terms of the flux contribution. The positive streamwise fluctuations, given by the Q1 and Q4 events, dominate the flow especially at the highest free-stream velocities (Fig. 7p). This is due to the drainage flow into the concave section which induces sweeps (Q4) towards the near-surface region as discussed above, and to the resulting displacement of high speed, colder fluid upwards (Q1) from the near-surface region as an effect of the stronger mixing occurring at the higher velocities. The outward interactions (Q1) can be therefore seen as bouncing flow resulting from preceding sweeps (Q4) directed towards the snow surface. This finds confirmation from the observation of outward interactions (Q1) at the higher tested free-stream velocity where the sweeps (Q4) are peaking closer to the snow surface, and by the relatively higher outward interactions (Q1) at X2 where the concave section allows the cold pool to form and as a consequence the mixing process to be stronger at the highest velocities. Thus, the inertial forces appear to be strong enough to mix most of the boundary layer within the cavity causing an enhancement of turbulent fluxes of momentum and heat close to the wall. At the deepest point of the cavity, however, the turbulent mixing is still suppressed within a very shallow layer at the wall and the concave surface still allows cold-air pooling.

These experiments were conducted for meteorological conditions typically observed over patchy snow covers, when the temperature difference between the snow surface and the ambient air typically ranges up to 15 °C causing low Richardson numbers ($Ri_b < 0.25$) meaning that the flow is dynamically unstable. Wind tunnel studies performed by Ohya (2001) and Ohya et al. (2008) over a flat cooled surface demonstrated that a significantly stronger atmospheric stability (Richardson number larger than 1) results in a suppression of momentum and heat fluxes over the whole boundary layer depth. In contrast to Ohya (2001) and Ohya et al. (2008), our wind tunnel studies show that only in the case of a flow with a low free stream wind velocity crossing a concavely shaped snow patch promotes the suppression of momentum and heat fluxes within the lowest part of the atmospheric boundary layer that is within the subjet layer.

TCD
9, 5413–5443, 2015

4 Conclusions

Wind tunnel experiments on flow development over a melting snow patch were conducted for meteorological conditions typically observed over patchy snow covers and strong snow melt in alpine environments. For the first time experiments were conducted to explore the relative role of topography vs. pure thermo-dynamics in causing atmospheric decoupling over a snow field. The experiments give evidence that topography is critical for the process of atmospheric decoupling by significantly altering the near-surface flow field. While the stability had a minor effect on flow dynamics over the flat snow field, it strongly influenced the near-surface flow behavior over the concavely shaped snow patch, especially if the free-stream wind velocity was low. For that experimental setup, the near-surface suppression of turbulence was observed to be strongest and drainage flows were decoupled from the surface enhancing atmospheric stability and promoting the cold-air pooling over the single snow patch. At higher wind velocities, the drainage flow was measured much closer to the surface causing a rush-in of high-momentum fluid of the outer layer to the wall region and an enhancement of turbulent mixing there. In the subjet layer, however, a very shallow layer characterized by a suppression of turbulent mixing was still present. Over the flat snow patch, profiles with low free-stream wind speeds only involved a weak suppression of the turbulent mixing in a very shallow layer above the snow cover. Thus, the strong atmospheric decoupling and cold-air pooling over single snow patches appears to be promoted by the cooling effect of the snow causing the development of a stable internal boundary layer above the snow patch, but also by the sheltering effect of the cavity and by the drainage flows which develop over the slopes of the cavity.

Thus, only the special experimental conditions with a concavely shaped snow patch and low free-stream wind velocities allowed the development of vertical profiles of turbulence that are typical for very stable regimes (Mahrt, 2014), when the maxima of turbulence is reached in a layer only intermittently coupled to the surface. The strong stability, but also the sloping terrain enables the formation of low-level drainage flows, which are known to be a driving force for cold-air pooling (Daly et al., 2010). For high free-stream wind velocities, the inertia of the flow becomes strong enough to mix the boundary layer above the snow surface (also for concave setup) and to consequently inhibit the stagnation of cold air and associated boundary layer decoupling within the local depression.

The suppression of heat exchange between the snow surface and the air adjacent to the surface effectively slows down snow ablation in spring and promotes the stagnation of the cold air within topographical depressions covered by snow (Fujita et al., 2010). The process of cold-air pooling and atmospheric decoupling is, thus, an important process driving the survival of long-lasting snow patches or all-season snow and ice fields in alpine or cold environments. The experimental results confirm the field study performed by Mott et al. (2013) who observed a strong suppression of downward heat fluxes close to the snow surface during calm wind conditions indicating boundary layer decoupling. The measurements of Mott et al. (2013) were, however, only conducted over a concavely shaped snow patch and lacked simultaneous measurements over a flat snow patch. Furthermore, measurements of the vertical profiles of turbulence intensities that were conducted by a eddy-correlation system were restricted by the low possible number of three measurements points. Compared to field measurements, the experimental setup in the wind tunnel allowed a high vertical resolution of flux measurements and allowed us to account for the effect of the topography on the flow development and the generation of turbulence in atmospheric layer adjacent to the snow.

The quantitative contribution of the atmospheric decoupling over melting snow for the total mass- and energy balance of a complete alpine catchment is not yet known. Although first numerical results of Mott et al. (2015) show that the interaction between boundary layer flow and fractional snow cover significantly affects the total energy balance, field measurements conducted over a larger area and for a complete melt season are necessary to estimate the relative frequency of phenomena enhancing (advective heat transport) or slowing down (atmospheric decoupling) snow melt. Such a compre-

TCD
9, 5413–5443, 2015

hensive experimental study is currently conducted in a three-years project in an alpine catchment in the Swiss Alps. Extensive field experiments during the entire ablation period are expected to provide new insight into the frequency of described phenomena and the importance for the snow hydrology of the total catchment.

Acknowledgements. The work presented here is supported by the Swiss National Science foundation SNF (Grant: 200021_150146).

References

Adrian, R. J., Meinhart, C. D., and Tomkins, C. D.: Vortex organization in the outer region of the turbulent boundary layer, J. Fluid Mech., 422, 1–54, 2000. 5424

Bodine, D., Klein, P., Arms, S., and Shapiro, A.: Variability of surface air temperature over gently sloped terrain, J. Appl. Meteorol., 48, 1117–1141, 2009. 5415

Burns, P. and Chemel, C.: Evolution of cold-air-pooling processes in complex terrain, Bound.-Lay. Meteorol., 150, 423–447, doi:10.1007/s10546-013-9885-z, 2014. 5415

Collis, D. C., and Williams, M. J.: Two-domensional convection from heated wires at low Reynolds numbers, J. Fluid Mech., 6, 357–384, doi:10.1017/S0022112059000696, 1959. 5419

Dadic, R., Mott, R., Lehning, M., and Burlando, P.: Wind influence on snow depth distribution and accumulation over glaciers, J. Geophys. Res., 115, F01012, doi:10.1029/2009JF001261, 2010. 5415

Daly, C., Conklin, D. R., and Unsworth, M. H.: Local atmospheric decoupling in complex terrain topography alters climate change impacts, Int. J. Climatol., 30, 1857–1864, doi:10.1002/joc.2007, 2010. 5428

Essery, R.: Modelling fluxes of momentum, sensible heat and latent heat over heterogeneous snowcover, Q. J. Roy. Meteorol. Soc., 123, 1867–1883, 1997. 5414, 5415

Essery, R., Granger, R., and Pomeroy, J. W.: Boundary-layer growth and advection of heat over snow and soil patches: modelling and parameterization, Hydrol. Process., 20, 953–967, 2006. 5415, 5422

TCD
9, 5413–5443, 2015

Atmospheric boundary layer flow above a single snow patch

R. Mott et al.

Fujita, K., Hiyama, K., Iida, H., and Ageta, Y.: Self-regulated fluctuations in the ablation of a snow patch over four decades, Water Resour. Res., 46, W11541, doi:10.1029/2009WR008383, 2010. 5415, 5416, 5428

Granger, R. J., Pomeroy, J. W., and Essery, R.: Boundary-layer growth and advection of heat over snow and soil patches: field observations, Hydrol. Process., 20, 953–967, 2006. 5415

Gustavsson, T., Karlsson, M., Bogren, J., and Lindqvist, S.: Development of temperature patterns during clear nights, J. Appl. Meteorol., 37, 559–571, 1998. 5415

Lehning, M., Löwe, H., Ryser, M., and Raderschall, N.: Inhomogeneous precipitation distribution and snow transport in steep terrain, Water Resour. Res., 44, W09425, doi:10.1029/2007WR006544, 2008. 5415

Mahrt, L.: Stably stratified atmospheric boundary layers, Annu. Rev. Fluid Mech., 46, 23–45, 2014. 5427

Mott, R., Schirmer, M., Bavay, M., Grünewald, T., and Lehning, M.: Understanding snow-transport processes shaping the mountain snow-cover, The Cryosphere, 4, 545–559, doi:10.5194/tc-4-545-2010, 2010. 5415

Mott, R., Egli, L., Grünewald, T., Dawes, N., Manes, C., Bavay, M., and Lehning, M.: Micrometeorological processes driving snow ablation in an Alpine catchment, The Cryosphere, 5, 1083–1098, doi:10.5194/tc-5-1083-2011, 2011. 5416, 5417

Mott, R., Gromke, C., Grünewald, T., and Lehning, M.: Relative importance of advective heat transport and boundary layer decoupling in the melt dynamics of a patchy snow cover, Adv. Water Resour., 55, 88–97, doi:10.1016/j.advwatres.2012.03.001, 2013. 5415, 5416, 5418, 5428

Mott, R., Scipión, D. E., Schneebeli, M., Dawes, N., and Lehning, M.: Orographic effects on snow deposition patterns in mountainous terrain, J. Geophys. Res.-Atmos., 119, 1419–1439, doi:10.1002/2013JD019880, 2014. 5415

Mott, R., Daniels, M., and Lehning, M.: Atmospheric flow development and associated changes in turbulent sensible heat flux over a patchy mountain snow cover, J. Hydrometeorol., 16, 1315–1340, doi:10.1175/JHM-D-14-0036.1, 2015. 5415, 5416, 5428

Neumann, N. and Marsh, P.: Local advection of sensible heat in the snowmalt landscape of Arctic tubdra, Hydrol. Process., 12, 1547–1560, 1998. 5415

Ohya, Y.: Wind-tunnel study of atmospheric stable boundary layers over a rough surface, Bound.-Lay. Meteorol., 98, 57–82, doi:10.1023/A:1018767829067, 2001. 5416, 5426

Ohya, Y.: Intermittent bursting of turbulence in a stable boundary layer with low-level jet, Bound.-Lay. Meteorol., 126, 349–363, doi:10.1007/s10546-007-9245-y, 2008. 5416, 5426

Price, J. D., Vosper, S., Brown, A., Ross, A., Clark, P., Davies, F., Horlacher, V., Claxton, B., McGregor, J. R., Hoare, J. S., Jemmett-Smith, B., and Sheridan, P.: COLPEX: field and numerical studies over a region of small hills, B. Am. Meteorol. Soc., 92, 1636–1650, 2011. 5415

Tabler, R. D.: Predicting profiles of snowdrifts in topographic catchments, in: Proceedings 43, Western Snow Conference, 23–25 April 1975, Coronado, Calif., 87–97, 1975. 5415

Vosper, S. B., Hughes, J. K., Lock, A. P., Sheridan, P. F., Ross, A. N., Jemmett-Smith, B., and Brown, A. R.: Cold-pool formation in a narrow valley, Q. J. Roy. MeteorOL. Soc., 140, 699–714, doi:10.1002/qj.2160, 2014. 5415

Wallace, J. M., Eckelmann, H., and Brodkey, R. S.: The wall region in turbulent shear flow, J. Fluid Mech., 54, 39–48, 1972. 5419

Whiteman, C. D., Zhong, S., Shaw, W. J., Hubbe, J. M., Bian, X., and Mittelstadt, J.: Cold pools in the Columbia Basin, Weather Forecast., 16, 432–447, 2001. 5415

Whiteman, C. D., Muschinski, A., Zhong, S., Fritts, D., Hoch, S. W., Hahnenberger, M., Yao, M., Hohreiter, V., Behn, M., Cheon, Y., Clements, C. B., Horst, T. W., Brown, W. O. J., and Oncley, S. P.: METCRAX: meteorological experiments in Arizonas meteor crater, B. Am. Meteorol. Soc., 89, 1665–1680, 2008. 5415

Winstral, A., Elder, K., and Davis, R. E.: Spatial snow modeling of wind-redistributed snow using terrain-based parameters, J. Hydrometeorol., 3, 524–538, 2002. 5415

TCD

9, 5413–5443, 2015

Atmospheric boundary layer flow above a single snow patch

R. Mott et al.

Table 1. Experimental setup for six atmospheric profiles with ambient wind velocity V_∞ ($\mathrm{m\,s^{-1}}$), fetch distance over the snow patch X_s (m), the bulk Richardson number Ri_bulk and the temperature difference between the surface and the ambient air temperature $\delta\theta$ (°C). The labels of profiles refer to their position ($X = X_\mathrm{s}$), ambient wind velocity ($U = U_\infty$) and the shape of the snow surface (c = concave, f = flat).

Profile	U_∞	X_s	Ri_bulk	$\delta\theta$
$\mathrm{E1}_{\mathrm{X1,V1}}$	0.96	+0.4	0.21	8.6
$\mathrm{E1}_{\mathrm{X2,V1}}$	0.98	+0.8	0.22	9.2
$\mathrm{E1}_{\mathrm{X1,V2}}$	1.94	+0.4	0.05	9.5
$\mathrm{E1}_{\mathrm{X2,V2}}$	2.03	+0.8	0.05	9.5
$\mathrm{E1}_{\mathrm{X1,V3}}$	3.2	+0.4	0.02	8.6
$\mathrm{E1}_{\mathrm{X2,V3}}$	3.33	+0.8	0.02	8.5
$\mathrm{E2}_{\mathrm{X1,V1}}$	0.94	+0.4	0.19	12.6
$\mathrm{E2}_{\mathrm{X2,V1}}$	0.91	+0.8	0.20	12.5
$\mathrm{E2}_{\mathrm{X1,V2}}$	1.93	+0.4	0.04	14.0
$\mathrm{E2}_{\mathrm{X2,V2}}$	1.8	+0.8	0.04	13.9
$\mathrm{E2}_{\mathrm{X1,V3}}$	2.84	+0.4	0.02	13.0
$\mathrm{E2}_{\mathrm{X2,V3}}$	2.84	+0.8	0.02	12.6

TCD
9, 5413–5443, 2015

TCD
9, 5413–5443, 2015

Atmospheric boundary layer flow above a single snow patch

R. Mott et al.

Table 2. Description of the categorization of fluid motions according to signs of u and w.

Sign of u	Sign of w	Sign of uw	Type of motion
+	+	+	Interaction outward Q1
−	+	−	Ejections Q2
−	−	+	Interaction (wallward) Q3
+	−	−	Sweeps Q4

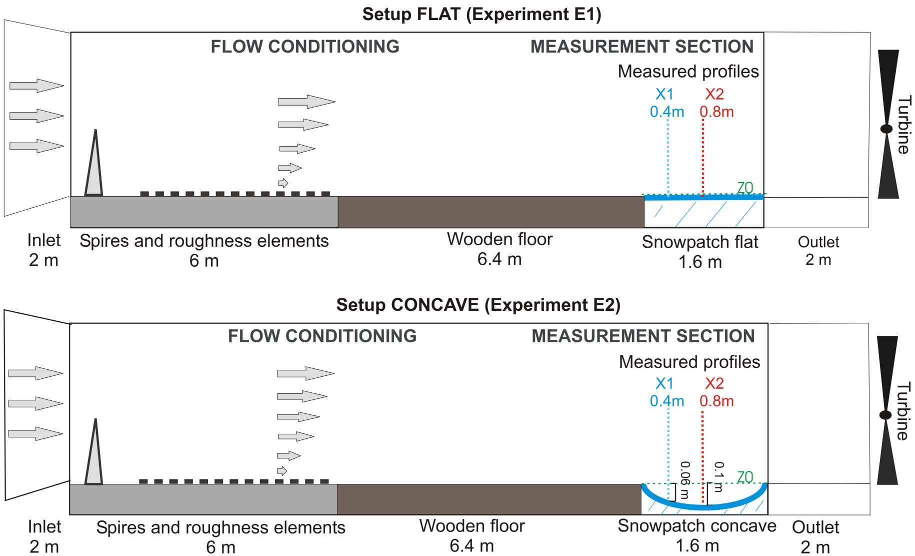

Figure 1. Sketch of the SLF boundary layer wind tunnel and measurement setup of experiments 1 (flat setup, E1) and experiment 2 (concave setup, E2). Measurement positions X are given relative to the leading edge of the snow patch with X0 = −0.1 m, X1 = 0.4 m and X2 = 0.8 m. Z0 marks the height of the step in topography for the concave setup (E2). Note that all heights z used in the following figures are relative to the height of the topographical step Z0. Consequently for the concave setup, the local surface at X1 correponds to $z = -0.06$ m and at X2 to $z = -0.1$ m.

TCD
9, 5413–5443, 2015

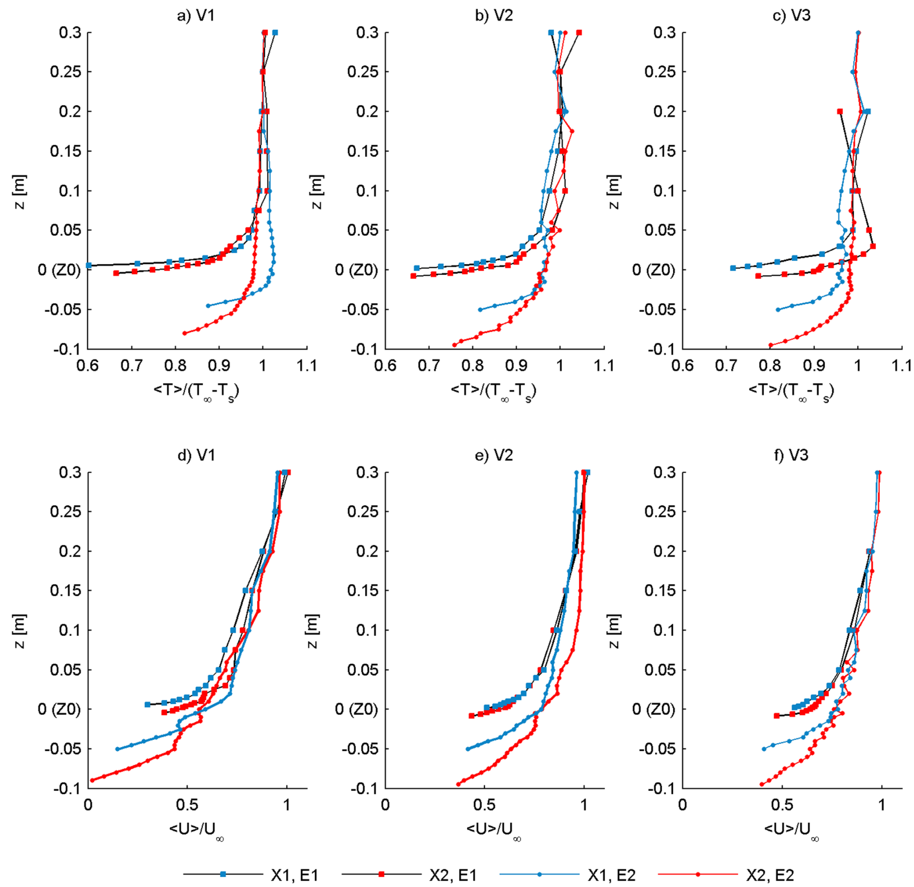

Figure 2. Vertical profiles of the mean air temperature and wind velocity normalized by the free stream temperature/wind velocity. Z0 marks the height of the topographical step at $z = 0$ m.

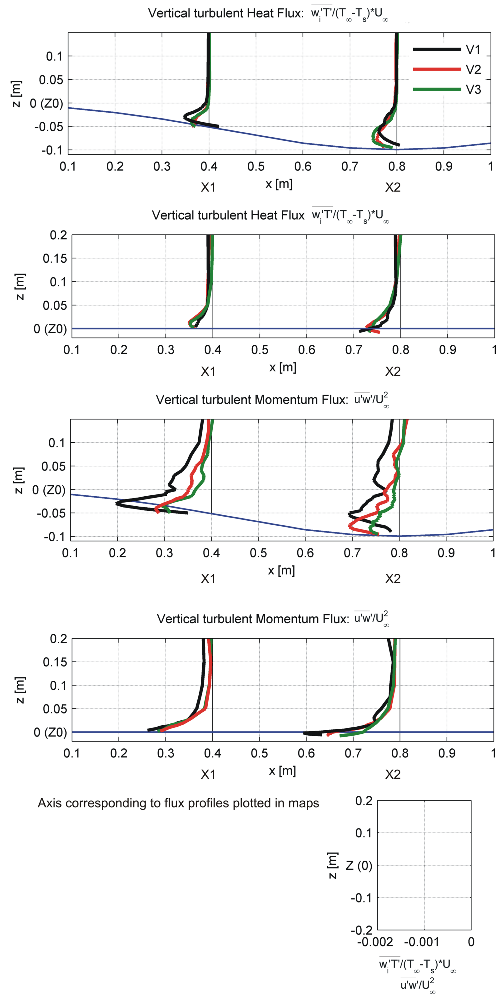

Vertical turbulent Heat Flux: w'T'/(T∞-Ts)*U∞
V1
V2
V3
z [m]
0.1
0.05
0 (Z0)
-0.05
-0.1
0.1 0.2 0.3 0.4 0.5 0.6 0.7 0.8 0.9 1
x [m]
X1
X2
Vertical turbulent Heat Flux w'T'/(T∞-Ts)*U∞
0.2
0.15
Vertical turbulent Momentum Flux: u'w'/U∞²
Vertical turbulent Momentum Flux: u'w'/U∞²
Axis corresponding to flux profiles plotted in maps
Z (0)
-0.2
-0.002 -0.001 0
w'T'/(T∞-Ts)*U∞
u'w'/U∞²

Figure 3. Vertical profiles of the turbulent fluxes: momentum flux $u'w'$ and turbulent vertical heat flux $w'\theta'$ normalized by the temperature difference and free stream wind velocity, plotted at the corresponding measurement location along the snow patch for the flat and concave setups. Z0 marks the height of the topographical step at $z = 0$ m. The axis corresponding to the flux profiles is plotted outside of the individual plots.

TCD
9, 5413–5443, 2015

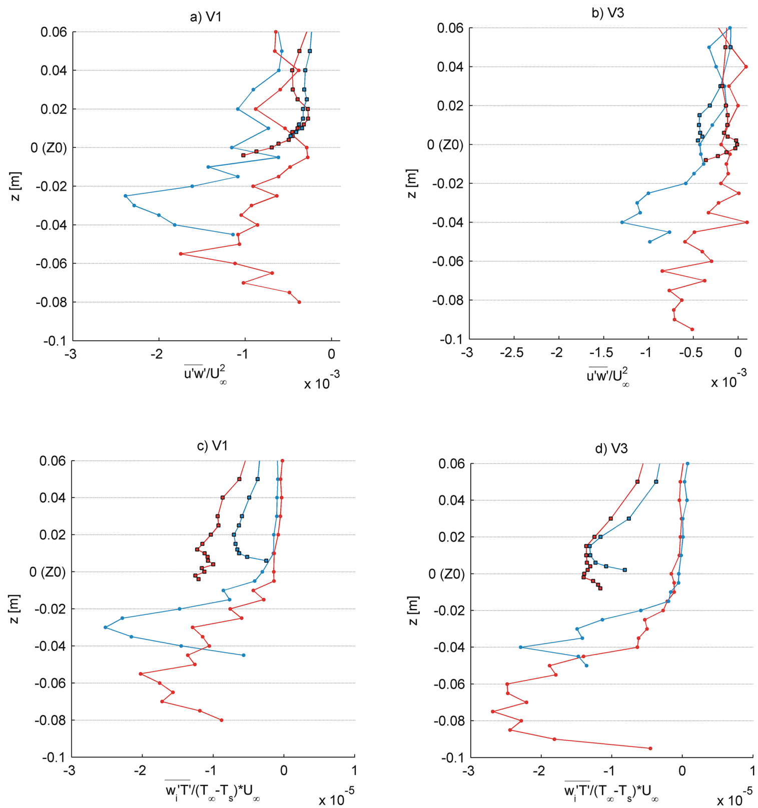

Figure 4. Vertical profiles of the turbulent fluxes: momentum flux $u'w'$ **(a, b)** and vertical heat flux $w'\theta'$ **(c, d)** normalized by the temperature difference and free stream wind velocity. Z0 marks the height of the topographical step at $z = 0$ m.

TCD
9, 5413–5443, 2015

Atmospheric boundary layer flow above a single snow patch

R. Mott et al.

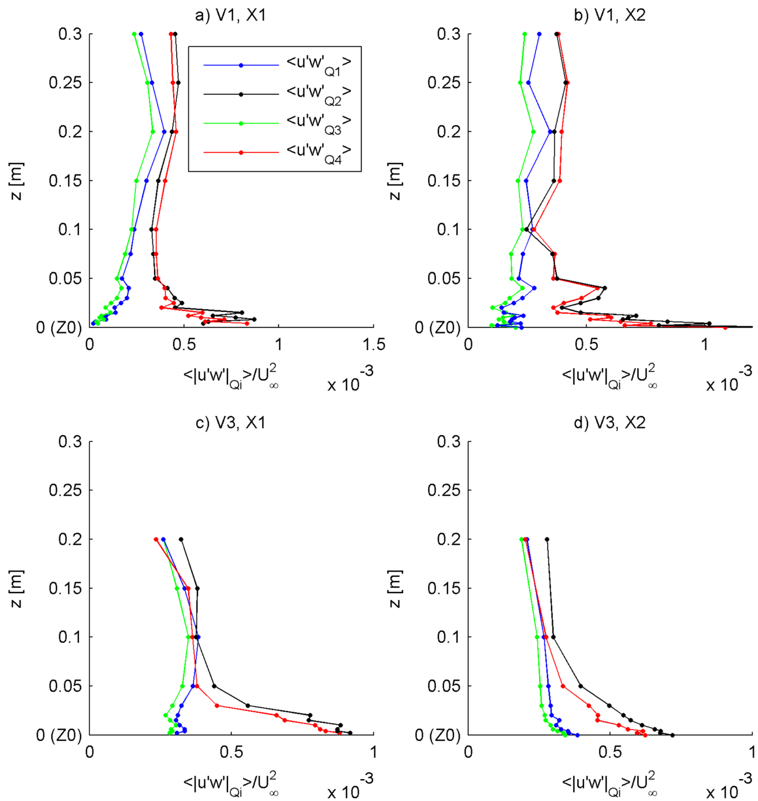

Figure 5. Shear stress contribution of the quadrants for the experimental setups E1V1 and E1V3.

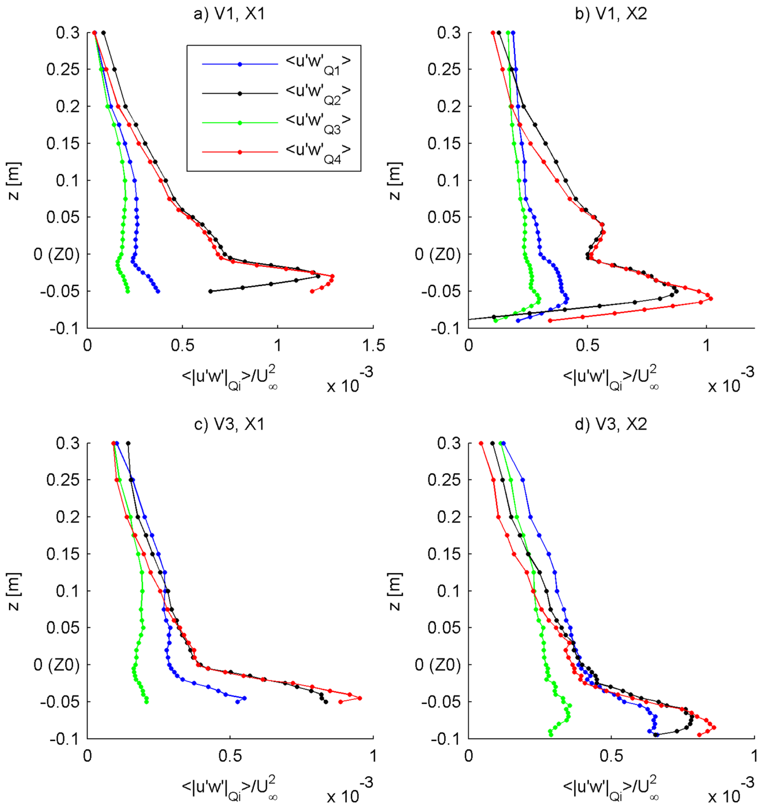

Figure 6. Shear stress contribution of the quadrants for the experimental setups E2V1 and E2V3.

TCD
9, 5413–5443, 2015

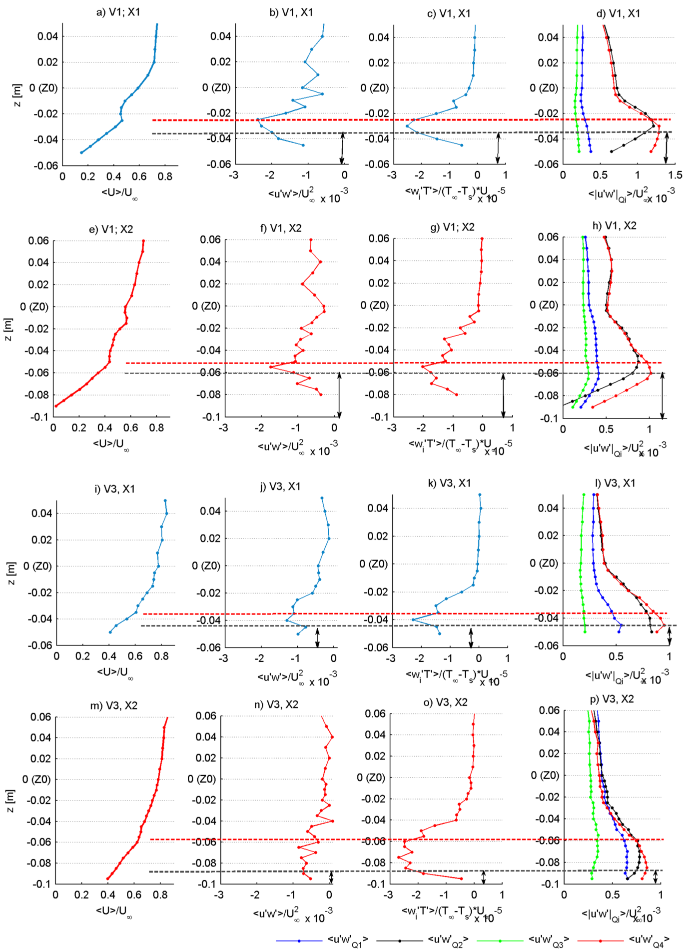

TCD
9, 5413–5443, 2015

Atmospheric boundary layer flow above a single snow patch

R. Mott et al.

Figure 7. Near-surface vertical profiles of mean wind speed, turbulent momentum flux, turbulent heat flux and shear stress distribution over the concave snow patch for experiment E2V1 at measurement location X1 **(a–d)** and at X2 **(e–h)** and for experiment E2V3 at X1 **(i–l)** and at X2 **(m–p)**. Z0 marks the height of the topographical step at $z = 0$ m. Red horizontal lines mark the area of local wind maxima indicating the nose of the low-level jet. Horizontal black lines indicate the upper limit of the near-surface suppression of turbulence.The black double-arrow mark the layer, where near-surface turbulence appears to occur.

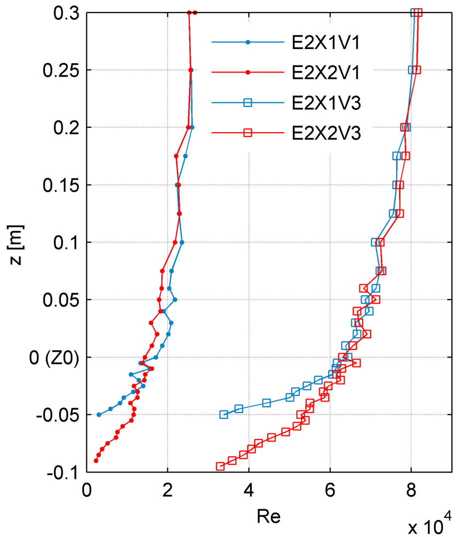

Figure 8. Vertical profiles of the Reynoldsnumber *Re* calculated from the local wind velocity at the respective measurement point.